Nuclear Engineering and Technology 55 (2023) 1009–1014

Contents lists available at ScienceDirect

Nuclear Engineering and Technology

journal homepage: www.elsevier.com/locate/net

Original Article

Development of a muon detector based on a plastic scintillator and WLS fibers to be used for muon tomography system

Chanwoo Park [a], Kyu Bom Kim [b], Min Kyu Baek [a], In-soo Kang [a], Seongyeon Lee [a], Yoon Soo Chung [a], Heejun Chung [c], Yong Hyun Chung [a, *]

[a] Department of Radiation Convergence Engineering, Yonsei University, Wonju, Republic of Korea
[b] Department of Integrative Medicine, Major in Digital Healthcare, Yonsei University College of Medicine, Seoul, Republic of Korea
[c] Korea Institute of Nuclear Nonproliferation and Control, Daejeon, Republic of Korea

ARTICLE INFO

Article history:
Received 17 January 2022
Received in revised form
25 October 2022
Accepted 21 November 2022
Available online 24 November 2022

Keywords:
Muon detector
Plastic scintillator
Wavelength-shifting fiber
Muon tomography

ABSTRACT

Muon tomography is a useful method for monitoring special nuclear materials (SNMs) such as spent nuclear fuel inside dry cask storage. Multiple Coulomb scattering of muons can be used to provide information about the 3-dimensional structure and atomic number(Z) of the inner materials. Tomography using muons is less affected by the shielding material and less harmful to health than other measurement methods.

We developed a muon detector for muon tomography, which consists of a plastic scintillator, 64 long wavelength-shifting (WLS) fibers attached to the top of the plastic scintillator, and silicon photomultipliers (SiPMs) connected to both ends of each WLS fiber. The muon detector can acquire X and Y positions simultaneously using a position determination algorithm.

The design parameters of the muon detector were optimized using DETECT2000 and Geant4 simulations, and a muon detector prototype was built based on the results. Spatial resolution measurement was performed using simulations and experiments to evaluate the feasibility of the muon detector. The experimental results were in good agreement with the simulation results. The muon detector has been confirmed for use in a muon tomography system.

1. Introduction

As the use of nuclear material in various industries increases, the importance of nuclear material monitoring is growing significantly. In order to prevent nuclear terrorism, a method of monitoring nuclear material must be accompanied [1].

Various technologies have been developed to monitor nuclear material. One of the methods is to measure the radiation emitted from nuclear material, such as portal monitoring, and the other is to measure the induced or transmitted radiation by irradiating the nuclear material, such as neutron activation analysis, X-ray backscatter imaging and multi-energy X-ray imaging. However, there are limitations in low detection efficiency and usage of artificial radiation sources [1–4].

In a previous study a simulated muon tomography system was designed and optimized for monitoring nuclear material, especially spent fuel inside dry storage containers [11]. Muon tomography utilizes the naturally occurring cosmic rays, therefore minimizing unwanted exposures from artificial radiation sources. By using high-energy muon that penetrates deep into the object, it is less affected by the shielding materials of the dry storage container. Also, the 3-dimensional structure of the inner material can be identified using multiple Coulomb scattering interactions of muons within the material.

The purpose of this study is to develop a muon detector for proof-of-concept based on a plastic scintillator and a wavelength-shifting (WLS) fiber for muon tomography, and to evaluate the feasibility of the developed muon detector. The muon detector was designed to detect two-dimensional positions of muon while reducing the number of photo-sensors and WLS fiber. WLS fibers were arranged in a line on the top of the scintillator and two silicon photomultipliers (SiPMs) were connected to both ends of each WLS fiber. The scintillation photons are absorbed by the WLS fiber and the re-emitted photons from the WLS fiber are detected by the two

* Corresponding author. 1 Yonseidae-gil, Wonju, Gangwon, 26493, Republic of Korea.
E-mail address: ychung@yonsei.ac.kr (Y.H. Chung).

https://doi.org/10.1016/j.net.2022.11.016

SiPMs. The X position of muon interaction is determined by comparing the number of photons detected between the WLS fibers, and the Y position is calculated by comparing the signals between the two SiPMs attached to both ends of the WLS fiber. It is possible to detect the X and Y-positions simultaneously with one detector, and the number of photo-sensors and WLS fibers could be reduced.

The muon detector, signal processing circuit, data acquisition system, and housing were built based on Monte-Carlo simulations, and the muon detector performance was verified.

2. Materials and methods

2.1. Principle of Muon tomography

Muons are charged particles created by interactions of primary cosmic rays in the upper atmosphere. Muons interact with atoms as they pass through matter, resulting in multiple Coulomb scattering. Muon tomography uses a scattering angle that is proportional to the atomic number (Z) of the material [5,6]. By tracking the trajectory of the muon, the material can be identified [3–10]. Fig. 1 shows the principle of muon tomography.

For image reconstruction of muon tomography, the Point-of-Closest-Approach (PoCA) algorithm is used to find the intersection of the incoming and outgoing muon tracks to determine the position and scattering angle. The PoCA algorithm approximates the closest position obtained by least-squares fitting of the interaction in the detector, and calculates the scattering angle between the two fitted tracks. The shortest line between the tracks is calculated by finding the closest pair of points between the two lines. The mid-point of the line is considered the muon's scattering point [12,13].

2.2. Design of a muon detector

The muon detector for proof-of-concept consists of a plastic scintillator (500 × 500 mm^2), 64 thin and long WLS fibers (3 × 500 × 3 mm^3) attached to the top of the plastic scintillator, and SiPMs (3 × 3 mm^2) connected to both ends of each WLS fiber as shown in Fig. 2. The scintillation photon generated by the plastic scintillator is transmitted to the SiPMs via a WLS fiber that absorbs the photon and re-emits it at a wavelength of 500 nm. Fig. 3 is a schematic diagram demonstrating the transmission of scintillation photon generated by the proposed detector.

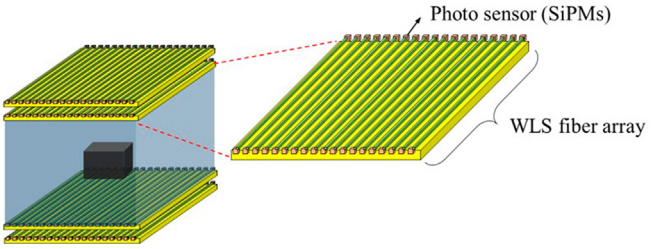

Fig. 2. Design of the proposed muon detector.

The proposed muon detector can acquire X and Y positions using a position determination algorithm (Fig. 4). The X position is determined by analyzing the photon distribution between WLS fibers using Anger logic [14]. Then, the Y position is calculated using the ratio between SiPMs attached to both ends of one WLS fiber.

In Fig. 4, the signals measured in SiPMs at both ends of the N_{th} WLS fiber were defined as SiPM a^n and SiPM b^n, respectively. The sum signal measured at the SiPMs of the N_{th} WLS fiber was defined as SiP$M_{total}M_{total}{}^n$. The X position can be found based on Anger logic by weighting the position of each WLS fiber according to signal strength, SiP$M_{total}M_{total}{}^n$, and then calculating the centroid position from the weighted positions as shown in Fig. 4(a). The Y position is determined by multiplying the ratio of SiPM a^n and SiP$M_{total}M_{total}{}^n$ and the length of the WLS fiber.

2.3. Optimization of a muon detector using simulation

DETECT2000 and Geant4 simulations were performed to optimize design parameters such as surface finish and scintillator thickness [15,16]. And the spatial resolution of the muon detector to which the optimized design parameters were applied was measured through simulation. The muon detector was simulated with a 500 × 500 mm^2 sized scintillator and 3 × 500 × 3 mm^3 sized 64 WLS fibers as described in the design of the muon detector.

Optimization of the surface treatment was performed using DETECT simulation as shown in Fig. 5. The measured light output from each WLS fiber depends on the surface treatment, which affects the spatial resolution of the detector. The light output was compared by applying the GROUND surface and the METAL surface with 0.98 refractive coefficient to the scintillator and WLS fiber.

Scintillator thickness optimization was performed using DETECT and Geant4 simulations. The scintillator thickness was varied as 1, 3, 5, 7, and 9 mm to analyze the difference in total light output measurement of all WLS fibers, and the detection efficiency of the muon detector.

The spatial resolution was performed by applying the optimized design parameters using DETECT simulation. Spatial resolution in simulation was measured using Sr-90 and Y-90, a daughter nucleus of Sr-90, a beta emission source that has similar characteristics to muon. The emitted beta ray has a continuous spectrum with a peak energy of 2.28 MeV, an energy similar to the average deposition

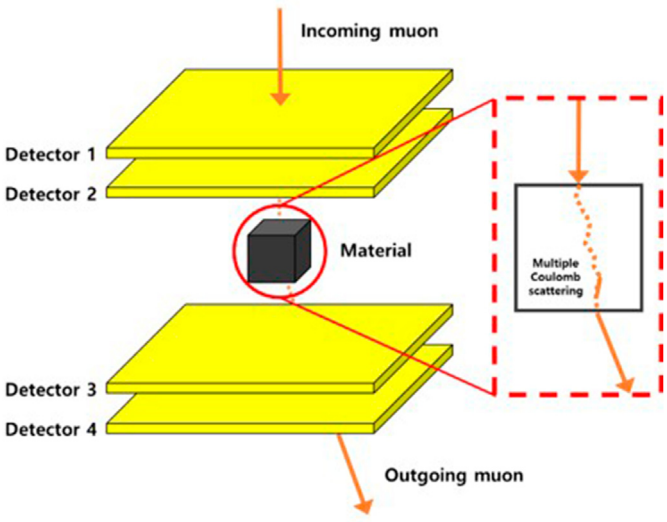

Fig. 1. The principle of muon tomography.

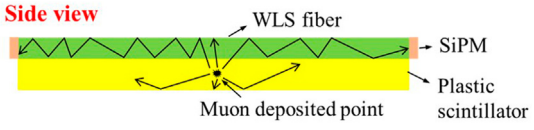

Fig. 3. Schematic diagram of muon interaction and its measurement.

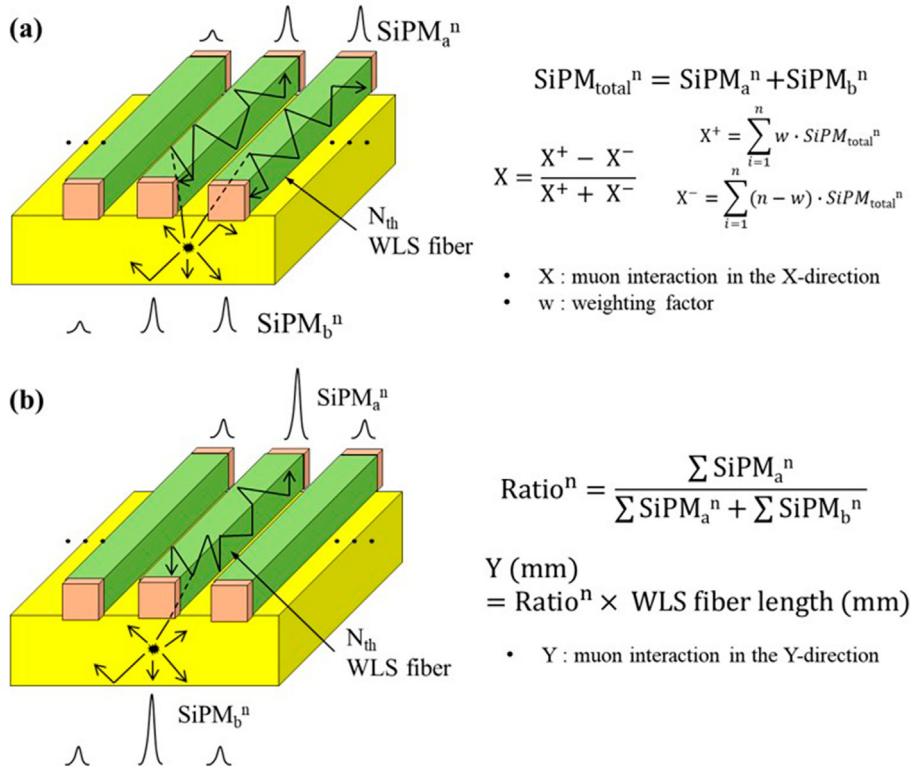

$$SiPM_{total}^{n} = SiPM_a^{n} + SiPM_b^{n}$$

$$X = \frac{X^+ - X^-}{X^+ + X^-} \qquad X^+ = \sum_{i=1}^{n} w \cdot SiPM_{total}^{n} \qquad X^- = \sum_{i=1}^{n} (n-w) \cdot SiPM_{total}^{n}$$

- X : muon interaction in the X-direction
- w : weighting factor

$$Ratio^n = \frac{\sum SiPM_a^n}{\sum SiPM_a^n + \sum SiPM_b^n}$$

$$Y\,(mm) = Ratio^n \times \text{WLS fiber length (mm)}$$

- Y : muon interaction in the Y-direction

Fig. 4. Position determination algorithm for muon detection.

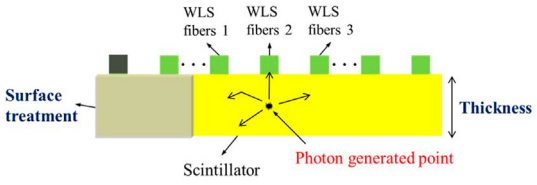

Fig. 5. Simulation geometry of a muon detector optimization.

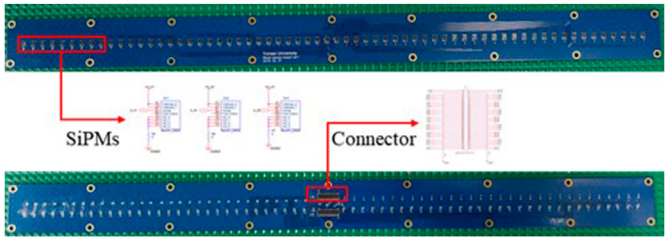

Fig. 6. Analog board for signal processing.

energy of a 3 GeV muon [17]. The detected photons measured at both ends of the WLS fibers were imaged using the position determination algorithm. Spatial resolution was measured through the full width at half maximum (FWHM) of the point profile in the resulting image.

2.4. Development of a muon detector

Based on the design and optimized parameters of the muon detector, a muon detector prototype was built, and spatial resolution was measured. A muon detector prototype consisting of a plastic scintillator (BC-408), WLS fibers (BCF-91A), and SiPMs (MICROFJ-30020-TSV-A1) were fabricated [18–20]. The optical grease, BC-630, was used to couple the WLS fibers to the scintillator and the SiPMs to the WLS fibers. Surface treatment was performed using Enhanced Specular Reflector (ESR) reflector.

The signal processing board and housing also were designed and manufactured. The signal processing board processes the signal measured by the SiPMs attached to the center of the board (Fig. 6). The detector housing which includes a plastic scintillator, WLS fibers, SiPMs, and signal processing board, was designed to block light.

The data acquisition system (DAQ) using TOFPET2 (PETsysElectronics) mainly consists of two parts: a front-end-module (FEM) and a front-end board D version 2 (FEB/D) [21]. Since FEM is a module with 64ch ASIC (Table 1), two FEM modules are required per a muon detector. FEB/D module connects a total of 16 FEMs and communicates with a computer.

Fig. 7 shows the fabricated muon detector combined with a plastic scintillator, 64 WLS fibers, ESR reflectors (METAL surface

Table 1
Characteristics of ASIC in FEM.

Characteristics	Value
Analog digital converter (ADC) Channel	64
ADC resolution	≥10 bit
ADC sampling rates	≥100 MHz
Time digital converter (TDC)Channel	64
TDC time binning	30 ps
Connection type	Ethernet

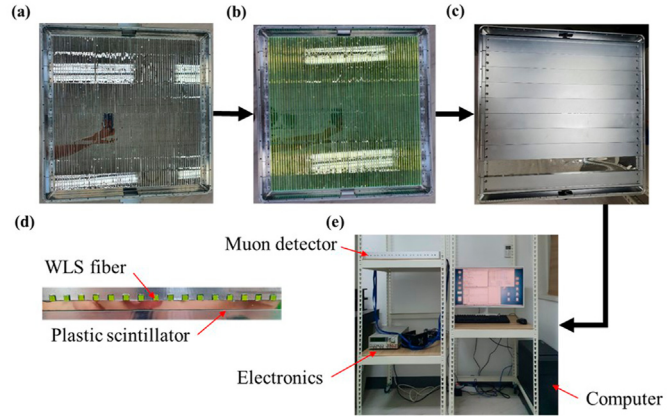

Fig. 7. Experimental setup of a muon detector (a) A detector housing with ESR reflectors, (b) A detector with a plastic scintillator and 64 WLS fibers, (c) Fastening the scintillator and fibers with housing, (d) Side view of the fabricated muon detector, (e) Experimental setup.

treatment), SiPMs, a signal processing board, and a detector housing.

Spatial resolution experiments were performed by placing a Sr-90 and Y-90 source with a pencil-beam collimator in the center of the muon detector. The spatial resolution was measured through the FWHM of the point profile from the experimental results. The performance of the fabricated muon detector was verified by comparing the measured spatial resolution with the DETECT simulation results.

3. Results

Surface treatment simulations were performed by changing the surface treatment of the scintillator and WLS fibers, respectively. The measured light outputs from WLS fibers 1, 2, and 3, where the photon generation location was below WLS fiber 2, were analyzed (Table 2). The highest light output was measured with the METAL treatment applied to both the scintillator and WLS fibers.

The total light output differences based on scintillator thickness variation simulations were performed. The total light output of the muon detector was measured using DETECT simulation, and the detection efficiency was measured using Geant4 simulation. As the scintillator thickness increases, the total light output decreases and the detection efficiency increases as shown in Fig. 8. Therefore, a scintillator thickness of 5 mm was determined as an optimized scintillator thickness with good detection efficiency and total light output.

The spatial resolution of the muon detector was measured by applying the optimized design parameters: METAL surface treatment and 5 mm scintillator thickness. The resulting image and the X and Y axis point profiles are shown in Fig. 9. The X and Y axis spatial resolutions were measured to be 3.9 mm and 4.5 mm, respectively.

The spatial resolution of a muon detector fabricated with optimized design parameters was experimentally measured using a Sr-90 source and a pencil-beam collimator. The point-like Sr-90 source was imaged using the position determination algorithm based on the same method used in the simulation. The X and Y axis spatial resolutions were measured to be 4.2 mm and 4.9 mm, respectively, as shown in Fig. 10.

Table 2
The simulation results of surface treatment.

Scintillator surface	WLS fiber surface	Fiber 1 (%)	Fiber 2(%)	Fiber 3(%)
METAL	METAL	4.21	9.37	4.05
	GROUND	3.87	8.95	3.92
GROUND	METAL	2.74	7.62	2.84
	GROUND	2.66	6.88	2.87

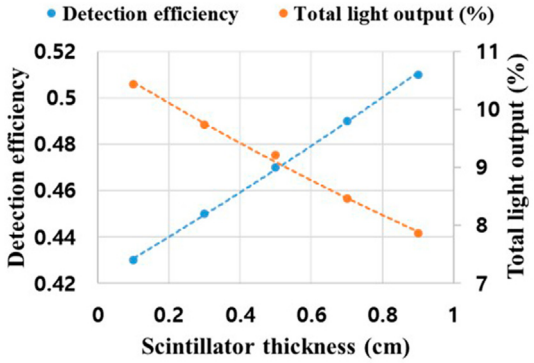

Fig. 8. Detection efficiency and total light output as a function of scintillator thickness.

4. Discussion & conclusion

The purpose of this study was to develop a muon detector based on a plastic scintillator and WLS fibers for the muon tomography system. A muon detector was designed and parameters such as surface treatment and scintillator thickness were optimized based on simulation results. Based on the optimized design parameters, a muon detector prototype was built using a plastic scintillator, WLS fibers, ESR reflectors, SiPMs, a signal processing board and a DAQ system. And, the performance of the developed muon detector was confirmed through the spatial resolution measurement experiment.

The plastic scintillator used in the developed muon detector has sufficient density and high light yield, so it has the advantage of relatively high detection efficiency. Thus, the detector for measuring muons was designed to utilize a large monolithic plastic scintillator. The newly designed muon detector has the advantage of simultaneously acquiring the X and Y positions through a single detector. In addition, there is an economic advantage because a relatively inexpensive plastic scintillator is used.

The performance of the developed muon detector was confirmed through the spatial resolution measurement experiment. As a result of the simulation using the Sr-90 source, the spatial resolution of the X and Y axes were predicted to be 3.9 mm and 4.5 mm, respectively. In the experiment, the spatial resolution of the X and Y axes were 4.2 mm and 4.9 mm, respectively.

The experimental results were analyzed with an error of about 10% compared to the simulation results. The difference in spatial resolution between simulation and experimental results is due to the difference in surface treatment. The amount of photons transmitted to the WLS fibers is reduced due to the inhomogeneity of the surface treatment. Also, the resolution difference occurred because the average beta energy of a Sr-90 source was used in the simulation. Therefore, the experimental results are considered to be consistent with the simulation results.

It was verified that the fabricated muon detector has feasibility as a detector of the muon tomography system. In future research, we plan to build a muon tomography system consisting of four muon detectors and to perform atomic number (Z) discrimination experiments on materials such as lead, iron, and aluminum.

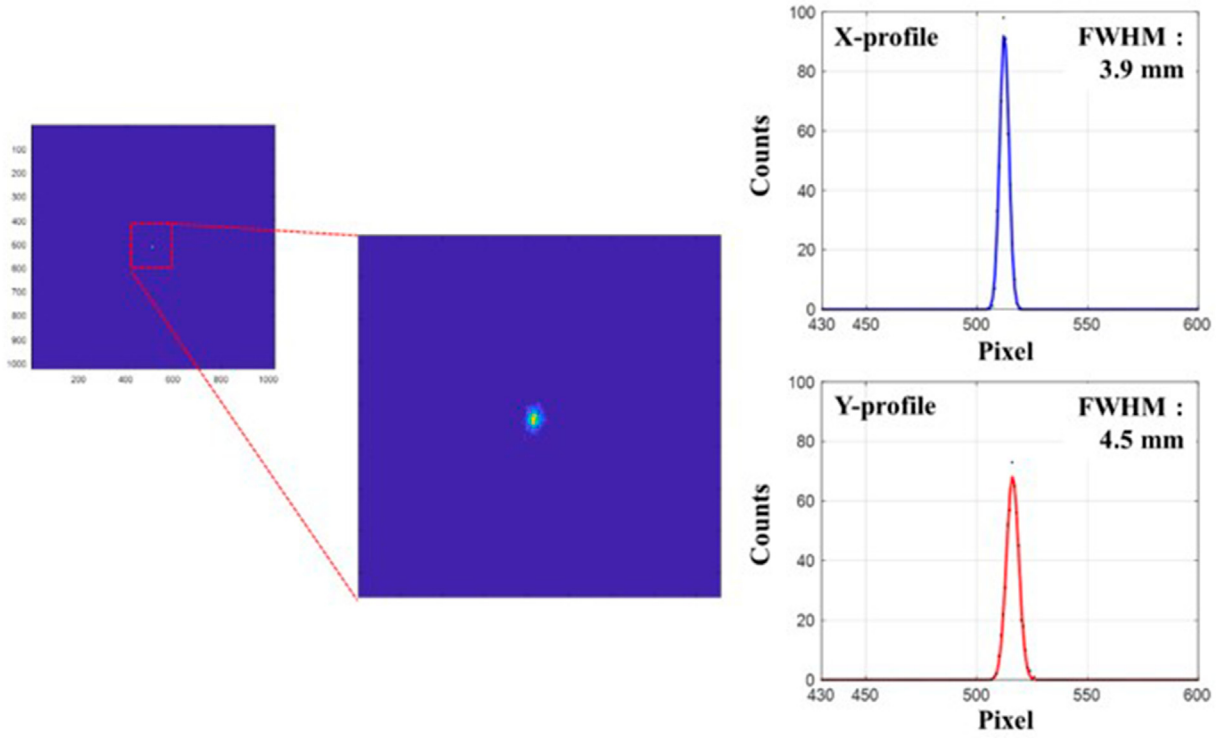

Fig. 9. Spatial resolution result using DETECT simulation.

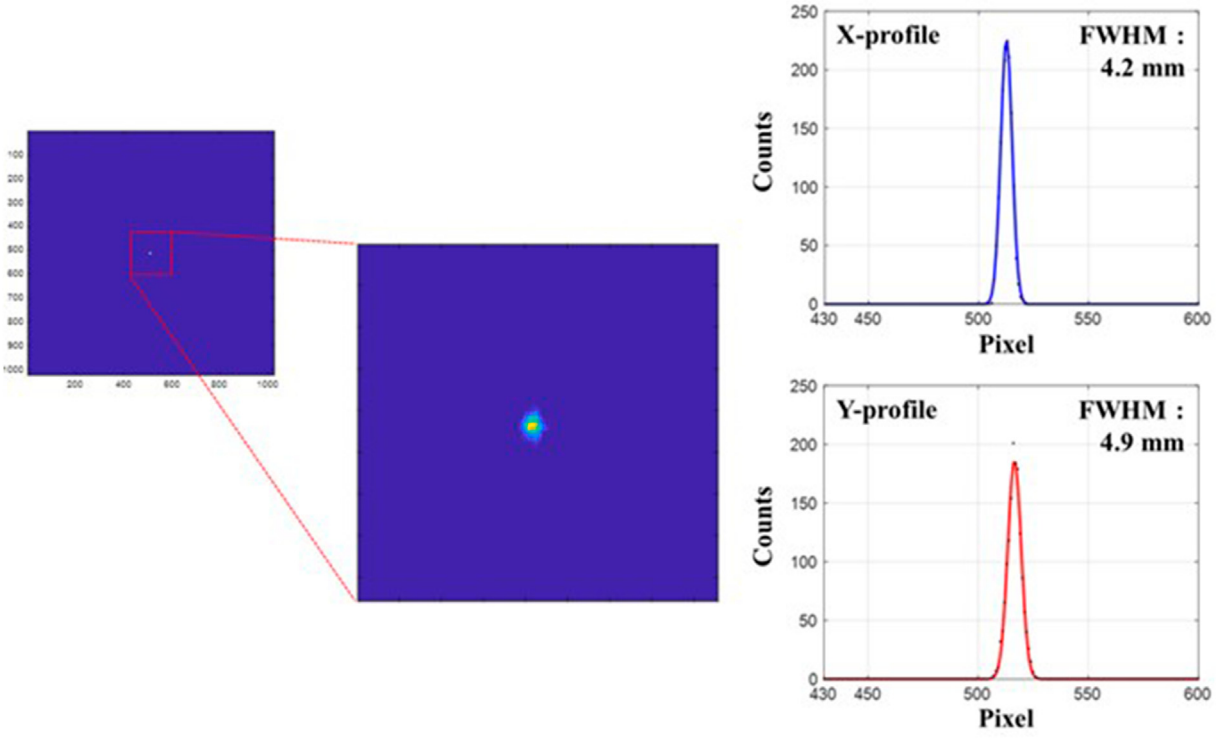

Fig. 10. Spatial resolution result using Sr-90 source.

Declaration of competing interest

The authors declare that they have no known competing financial interests or personal relationships that could have appeared to influence the work reported in this paper.

Acknowledgements

This work was supported by the Nuclear Safety Research Program through the Korea Foundation Of Nuclear Safety (KoFONS) using the financial resource granted by the Nuclear Safety and Security Commission (NSSC) of the Republic of Korea. (No. 1804025).

References

[1] J. Medalia, Detection of Nuclear Weapons and Materials: Science, Technologies, Observations, CRS Report for Congress, 2009, R40154.
[2] R.C. Runkle, A. Bernstein, P. Vanier, Securing special nuclear material: recent advances in neutron detection and their role in nonproliferation, J. Appl. Phys. 108 (2010), 111101.
[3] M. Hohlmann, P. Ford, K. Gnanvo, et al., GEANT4 simulation of a cosmic ray muon tomography system with micro-pattern gas detectors for the detection of high-Z materials, IEEE Trans. Nucl. Sci. 56 (3) (2009) 1356–1363.
[4] G. Bonomi, Progress in Muon Tomography, EPS Conference on High Energy Physics, 2017. Venice, Italy.
[5] D. Poulson, J.M. Durham, E. Guardincerri, et al., Cosmic ray muon computed tomography of spent nuclear fuel in dry storage casks, Nucl. Instrum. Methods Phys. Res. 842 (48–53) (2017).
[6] J. Matthew Durham, Elena Guardincerri, Christopher L. Morris, Daniel Poulson, et al., Cosmic ray muon imaging of spent nuclear fuel in dry storage casks, J. Nucl. Mater. Manag. 44 (3) (2016).
[7] J.M. Durham, D. Poulson, et al., Verification of spent nuclear fuel in sealed dry storage casks via measurements of cosmic-ray muon scattering, Phys. Rev. Applied 9 (2018), 044013.
[8] S. Pesente, et al., First results on material identification and imaging with a large-volume muon tomography prototype, Nucl. Instrum. Methods A 604 (2009) 738–746.
[9] V. Anghel, A. Erlandson, D. Waller, et al., A plastic scintillator-based muon tomography system with an integrated muon spectrometer, Nucl. Instrum. Methods A 798 (2015) 12–23.
[10] Haruo Miyadera, L. Christopher, Morris, Muon scattering tomography: review, Appl. Opt. 61 (2022) 154–161.
[11] Chanwoo Park, Min Kyu Baek, In-soo Kang, Seongyeon Lee, Heejun Chung, Yong Hyun Chung, Design and Characterization of a Muon Tomography System for Spent Nuclear Fuel Monitoring, Nuclear Engineering and Technology, 2021.
[12] L.J. Schultz, et al., Image reconstruction and material Z discrimination via cosmic ray muon radiography, Nucl. Instrum. Methods A 519 (2004) 687.
[13] M. Durham, Cosmic Ray Muon Tomography, 2016. https://permalink.lanl.gov/object/tr?what=info:lanl-repo/lareport/LA-UR-16-27760.
[14] H.O. Anger, Scintillation camera, Rev. Sci. Instrum. 29 (27) (1958).
[15] C. Moisan, F. Cayouet, G. McDonald, DETECT 2000, the Object Oriented C++ Language Version of DETECT, Laval University, Canada, 2000.
[16] S. Agostinelli, et al., GEANT4 - a simulation toolkit, Nucl. Instrum. Methods Phys. Res., Sect. A 506 (3) (2003) 250–303.
[17] S. Arfaoui, Characterisation of a Sr-90 Based Electron Monochromator, CERN - European Organization for Nuclear Research, 2015.
[18] Saint gobain. BC-400, BC-404, BC-408, BC-412, BC-416 premium plastic scintillators. https://www.crystals.saint-gobain.com/sites/imdf.crystals.com/files/documents/bc400-404-408-412-416-data-sheet.pdf.
[19] Saint gobain, Plastic Scintillating Fibers, 2017. https://www.crystals.saint-gobain.com/sites/imdf.crystals.com/files/documents/fiber-product-sheet.pdf.
[20] onsemi, Silicon Photomultipliers (SiPM), High PDE and Timing Resolution Sensors in a TSV Package - J-Series SiPM Sensors, 2017. https://www.onsemi.com/pdf/datasheet/microj-series-d.pdf.
[21] PETsys Electronics, TOFPET2 ASIC Evaluation Kit Hardware User Guide (v1.3), 2018.